



Modeling of pile-soil-pile interaction in laterally loaded pile groups embedded in linear elastic soil layers

Volkan Isbuga¹

Received: 18 November 2019 / Accepted: 21 February 2020 / Published online: 18 April 2020
© Saudi Society for Geosciences 2020

Abstract

This study proposes a new method to obtain the lateral response of pile groups by incorporating the pile group effect in layered soils. When a pile is loaded laterally, it creates a zone of influence in the direction of loading. In a pile group, each pile placed in the influence zone of prior piles is exposed to extra loads due to the load transfers from other piles. This mechanism results in a group effect which causes each pile in the group to have a different deflection curve compared to that of an identical isolated single pile under the same load. This study starts with a mathematical approach to model the interaction of two piles and then extends it to pile groups. The governing differential equation of a pile deflection problem is modified to take the pile-soil-pile interaction into account and solved analytically for each pile while the soil parameters and displacement fields around each pile are obtained numerically using the finite difference method written in Fortran language. The model captures the additional pile deflections induced by the group effects in pile groups and the results match well with the results of the existing methods, especially the finite element method.

Keywords Pile groups · Shadowing effect · Lateral group response · Pile-soil interaction

Introduction

Piles are often used when soil strength properties are not enough to sustain the loads from the superstructure. When loads are very high, piles are used in groups to meet a required load-carrying capacity. Pile groups may also experience strong lateral loads such as wind loads. If piles are closely spaced, lateral loads acting on the piles can be transferred to other piles via pile-soil-pile interactions in a group. One of the main parameters controlling the interaction among piles is the radial distance between piles. This interaction becomes especially significant for pile groups consisting of a large number of piles. If a pile is loaded laterally on top, it creates a displacement field, a zone of influence, in the direction of loading. The soil in this field will displace mainly in the direction of loading and the magnitude of displacements will be

inversely proportional to the distance from the loaded pile. These influence zones overlap in a pile group, and interactions transfer the loads to the next piles in line causing additional loads on piles. This mechanism is called group effect, also known as shadowing effect, that causes a reduction in the load-carrying capacity of each pile under anticipated load distribution in pile groups (Bonakdar and Oumeraci 2015; Giannakos et al. 2012; Heidari et al. 2014; Ilyas et al. 2004; McVay et al. 1996). There are several experimental and computational modeling attempts in the literature to capture the group effect in the response of pile groups. A broad review of earlier works in modeling the response of laterally loaded pile groups was presented by Duncan et al. (1994). Various researchers conducted field experiments or laboratory experiments to determine the group effect in laterally loaded piles (Brown et al. 1987; Guo et al. 2014; Matlock et al. 1980; McVay et al. 1996; Meimon et al. 1986; Moss et al. 1998). Computational methods vary, however, they can be simply classified as discrete models and continuum models. Discrete models represent soil layers with discrete springs, whereas continuum models take the continuous structure of soils into account.

Practitioners often time apply the p-y method to determine the response of pile groups to lateral loads. In the p-y method,

Responsible Editor: Zeynal Abiddin Erguler

✉ Volkan Isbuga
volkanisbuga@iyte.edu.tr

¹ Department of Civil Engineering, Izmir Institute of Technology, 35430 Izmir, Turkey

a load-deflection curve or load resistance determined by a single pile analysis is modified to account for group effect by a p -multiplier. Experimental works for this method mainly focuses on determining the p -multipliers, which denote load reduction parameters for each pile, depending on its location in the group. Then, the p -multipliers are used to scale down the load-deflection curve of a separate single pile and applied to each pile in the group (Abdrabbo and Gaaver 2012; Comodromos and Papadopoulou 2013; Duncan et al. 1994; McVay et al. 1995; Ooi et al. 2004; Rollins et al. 1998, 2006; Tahghighi and Konagai 2007). The main drawbacks of the experimental studies are the difficulty to simulate soil layers, which can vary for different sites, and model the pile groups with non-homogeneous pile distribution. Numerical works including the finite difference method (FDM) and the finite element method (FEM) also exist in the literature to analyze the pile groups or determine the p -multipliers (Bransby 1996; Brown and Shie 1991; Comodromos and Ptilakis 2005; Elhakim et al. 2016; Fan et al. 2007; Larsson et al. 2012; Law and Lam 2001; Papadopoulou and Comodromos 2010; Wu et al. 2015; Yang and Jeremić 2003). Especially, the finite element method has been often applied to analyze pile groups. Broad literature in constitutive models implemented in FEM software and the availability of FEM commercial software packages provide the opportunity to include the realistic behavior of soils through plasticity models. Although the finite element-based models are applicable to a wide range of problems and commercial software options are available for engineers, applying FEM in the design stage of a structure may require enormous computational source and time. It might include numerous runs and pre-/post-processing for large pile groups, especially with a non-uniform pile distribution (different pile spacings). The boundary element method (BEM) has been also used substantially to model piles and pile groups (Ai and Feng 2014; Ai and Li 2015; Ai et al. 2016; Banerjee and Driscoll 1976; Mamoon et al. 1990; Padron et al. 2007; Sen et al. 1985; Xu and Poulos 2000). Some recent significant contributions in the application of BEM have been introduced by Ai and Feng (2014), Ai and Li (2015), and Ai et al. (2016). The researchers analyzed laterally loaded pile groups placed in transversely isotropic soils by applying the boundary element method considering pile-soil-pile interaction, and also presented a framework of FEM-BEM coupling for pile group analysis under dynamic loads. Overall, the BEM was demonstrated as a strong and efficient method to be employed for pile group analyses by various researchers. Another numerical approach was proposed by Ashour et al. (2004) who evaluated the behavior of a pile group based on the strain wedge model to obtain the p - y curves of each pile in the group.

An important approach followed by researchers is the method based on beam on Winkler foundation (BWF) models (Bahrami and Nikraz 2017; Mylonakis and Gazetas 1999; Tahghighi and Konagai 2007). This method discretizes the

soil layers as linear springs and sometimes also with dash-pots (for dynamic problems to include damping), each of which represents a different type of soil layer along the pile shaft. The method has been used for single laterally loaded piles and also pile groups. It allows using the well-known differential equation of an elastic foundation on Winkler's springs for a single pile. Mylonakis and Gazetas (1999) employed it for determining the lateral vibration of laterally loaded pile groups. The researchers set up a model by starting with two piles in layered soils under a lateral load. To determine the deflection of the unloaded pile due to interaction forces, the soil displacements around the loaded pile was calculated by multiplying the pile deflection with an attenuation function since the soil displacements cannot be obtained directly from their single pile analysis.

Sun (1994) modeled a laterally loaded single pile embedded in a linear elastic medium by using the variational method. The model considers the continuous structure of the soil layer, which is the main difference between the BWF approach, and introduces an additional term appearing in the fourth-order differential equation of the pile deflection. The researcher obtained the solution for the pile deflection problem and proposed the relations for the displacement field of an elastic continuum around the pile. The application of variational principles to derive the governing equations for foundation-soil systems has been also presented as an alternative way by Aşık (1999) and Aşık and Vallabhan (2001) for a single footing under vertical excitation. Basu et al. (2009) assumed two different attenuation functions in radial and circumferential directions in the formulation proposed by Sun (1994). This new assumption resulted in two coupled differential equations to be solved for displacements rather than the single differential equation given by Sun (1994). Salgado et al. (2014) also applied variational principles and presented a solution algorithm including a complicated mathematical approach for laterally loaded pile groups. The work of Salgado et al. (2014) differs from this study in formulating the problem by applying the principle minimum potential energy and calculus of variations to whole pile group system and surrounding soil rather than extending the single pile-based solution. In a mathematical view, Salgado et al. (2014) accounted for soil displacements and decay functions all solved simultaneously in a coupled fashion, whereas the proposed approach in this study considers the interaction effect as a force term acting on piles, which yields a totally different mathematical solution method for obtaining pile deflections.

The interaction model proposed and applied by Mylonakis and Gazetas (1999), who employed it under dynamic loads for the soil layers presented by discrete springs, does not consider soil continuity and displacements around the pile being analyzed. This study follows a similar interaction idea but solves a different differential equation. The solution of the governing equation in this work and the way of calculating the

attenuation factors are based on totally different displacement assumptions and mathematical equations than those of Mylonakis and Gazetas (1999). The author of the present work developed a Fortran code, which makes use of the model in the literature for single piles proposed by Sun (1994) and the later modified version by Basu et al. (2009) for the solution of a laterally loaded single pile and extends these earlier works to pile groups by accounting for the new interaction model among the piles. Then, the mathematical model has been developed to account for the interaction effects among piles. This new approach introduces the application of the interaction idea to piles under static loads and embedded in continuous soils, formulates the mathematical model in conjunction with an iterative algorithm as described in Section “Interaction between two piles” to have consistent soil parameters with deflections caused by the interaction forces. The next section introduces the single pile model that is the basis for the pile groups model followed by the new interaction developed in this study and the extension to the pile groups with numerical examples.

Laterally loaded single pile

This section briefly mentions the previous method proposed by Sun (1994) and modified by Basu et al. (2009) for a laterally loaded single pile that forms a basis for this study to further extend it to pile groups. Following the single pile solution, the interaction model which is proposed by this study between two piles is introduced.

For a pile embedded in a linear elastic soil layer (Fig. 1), the displacements can be approximated by (Basu et al. 2009):

$$u_r = w(z)\phi_r(r)\cos\theta \tag{1}$$

$$u_\theta = -w(z)\phi_\theta(r)\sin\theta \tag{2}$$

$$u_z = 0 \tag{3}$$

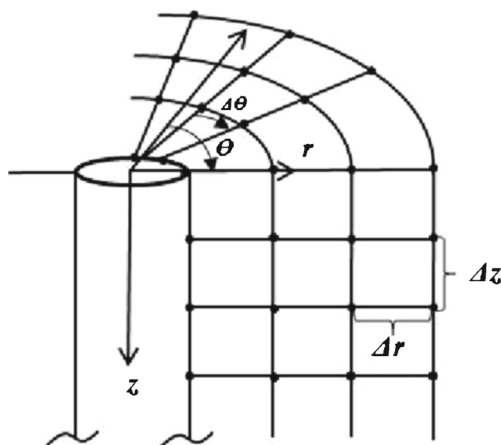


Fig. 1 Schematic numerical discretization of a pile and soil

where w is the pile deflection; u_r and u_θ are the radial and circumferential displacements, respectively, at any point in the soil medium around the pile; and u_z is the vertical displacement and assumed to be negligible for a laterally loaded pile, which is the interest of this work. $\phi_r(r)$ and $\phi_\theta(r)$ are the dimensionless attenuation displacement functions descending with the radial distance from the pile center, r is the radial coordinate, and θ is the angle measured from the radial axis as shown in Fig. 1. Equations. (1)–(3) produce a continuous displacement field around the pile.

The deflection of a single pile embedded in a continuous soil consisting of multiple layers can be expressed as:

$$\frac{\partial^4 \tilde{w}_i}{\partial \tilde{z}^4} - 2\tilde{t} \frac{\partial^2 \tilde{w}_i}{\partial \tilde{z}^2} + \tilde{k}_i \tilde{w}_i = 0 \tag{4}$$

where \tilde{w}_i is the normalized deflection of pile by the pile length L_p and defined for each layer as $\tilde{w}_i = w_i/L_p$, \tilde{z} is the depth and normalized by L_p , \tilde{t}_i and \tilde{k}_i are also the soil parameters of i th layer, which take the soil stiffness into account. \tilde{t} and \tilde{k} are normalized as $\tilde{t} = (tL_p^2)/(E_p J_p)$ and $\tilde{k} = (kL_p^4)/(E_p J_p)$, respectively. The solution of Eq. (4) is expressed as:

$$\tilde{w}_i(z) = C_1^i \Phi_1 + C_2^i \Phi_2 + C_3^i \Phi_3 + C_4^i \Phi_4 \tag{5}$$

C_j are the constant coefficients for each layer where $j = 1 \dots 4$ and to be found from BCs and continuity equations on the deflection, slope, moment, and shear force at interfaces of subsequent layers. Φ_j are known functions and defined as:

$$\Phi_1 = \sinh p_i \tilde{z} \cos q_i \tilde{z} \tag{6}$$

$$\Phi_2 = \cosh p_i \tilde{z} \cos q_i \tilde{z} \tag{7}$$

$$\Phi_3 = \cosh p_i \tilde{z} \sin q_i \tilde{z} \tag{8}$$

$$\Phi_4 = \sinh p_i \tilde{z} \sin q_i \tilde{z} \tag{9}$$

where p_i and q_i are, respectively, defined as:

$$p_i = \sqrt{\frac{\sqrt{\tilde{k}_i^{(1)}} + \tilde{t}_i^{(1)}}{2}} \tag{10}$$

$$q_i = \sqrt{\frac{\sqrt{\tilde{k}_i^{(1)}} - \tilde{t}_i^{(1)}}{2}} \tag{11}$$

Depending on the relation between \tilde{t} and \tilde{k} , the mathematical solution and definitions of Φ_i may vary. Here, the author assumed the case where $\tilde{k} > \tilde{t}^2$ throughout this work. The single pile solution requires the pile and soil to be discretized along the radial axis, circumferential axis, and also the vertical axis (see Fig. 1). A three-dimensional displacement field due to the lateral load on a pile can be obtained by Eqs. (1)–(3), which require the

two coupled differential equations to be solved numerically for $\phi_r(r)$ and $\phi_\theta(r)$. In this work, a band matrix solver routine is applied to solve these equations numerically. This modification increased the speed of the single pile model and made the method computationally more efficient to be further developed for pile group analyses. The solution of these coupled differential equations include the parameters γ_m where $m = 1 \dots 6$. These parameters depend on material properties of the soil and pile deflection directly. An iterative scheme is necessary to calculate γ_m since they involve the pile deflection term \tilde{w} . Although this parameter is a scalar value in Sun (1994), it becomes a set of six different parameters (γ_i) each of which consists of lengthy mathematical expressions depending on t and k in the work of Basu et al. (2009). The definitions of the soil parameters t and k , and also γ_i can be already found in those previous works; therefore, they will not be repeated here for the sake of simplicity. Readers are referred to those works for the detailed mathematical definitions of the parameters.

If we consider only a single layer and drop the subscript i for simplicity for a pile loaded by a normalized force $\tilde{F} = (FL_p)/(E_p I_p)$ at $z = 0$, the constants in Eq. (5) can be obtained from the BCs which are:

$$\left(\frac{\partial^3 \tilde{w}}{\partial \tilde{z}^3} - 2t \frac{\partial^2 \tilde{w}}{\partial \tilde{z}^2} \right) \Big|_{\tilde{z}=0} = \tilde{F} \tag{12}$$

Similarly, if there is also a moment M acting on the top of the pile where $\tilde{M} = \frac{ML_p}{E_p I_p}$

$$\left(\frac{\partial^3 \tilde{w}}{\partial \tilde{z}^3} \right) \Big|_{\tilde{z}=0} = \tilde{M} \tag{13}$$

and if the pile is fixed at ($\tilde{z} = 1$) the bottom end

$$\tilde{w} \Big|_{\tilde{z}=1} = 0 \tag{14}$$

$$\left(\frac{\partial \tilde{w}}{\partial \tilde{z}} \right) \Big|_{\tilde{z}=1} = 0 \tag{15}$$

However, the BCs can be changed to represent a floating pile with a rigid pile-cap, which requires to assign a displacement BC and no rotation (simulating a rigid cap) for the pile top and free-end BC at the bottom. For this case, BCs will be:

$$\tilde{w} \Big|_{z=0} = \tilde{w}_{top} \tag{16}$$

$$\frac{\partial \tilde{w}}{\partial \tilde{z}} \Big|_{z=0} = 0 \tag{17}$$

where \tilde{w}_{top} is a known pile-cap displacement. At ($\tilde{z} = 1$), the pile-tip BCs are:

$$\left(\frac{\partial^3 \tilde{w}}{\partial \tilde{z}^3} - 2t \frac{\partial^2 \tilde{w}}{\partial \tilde{z}^2} \right) \Big|_{\tilde{z}=1} = \sqrt{2kt\tilde{w}} \tag{18}$$

$$\left(\frac{\partial^2 \tilde{w}}{\partial \tilde{z}^2} \right) \Big|_{\tilde{z}=1} = 0 \tag{19}$$

Eq. (5) together with Eqs. (12)–(19) complete the solution of the differential equation of a single laterally loaded pile for the given BCs.

Interaction between two piles

This section follows the terminology used in previous studies (Loria et al. 2018; Mylonakis and Gazetas 1999; Randolph and Wroth 1979). First, we consider a pile group consisting of two closely spaced piles embedded in an elastic continuous medium. Then, the results for pile group consisting of various numbers of piles are presented in “Numerical examples.” The first pile, which has a force acting on its head, is called the “source” pile. The source pile is first analyzed with the assumption that the “receiver” pile (the second pile), on which no force acts, does not exist. Recall that the single-pile deflection problem is formulated assuming that soil displacements around the pile are represented by displacement functions given in Eqs. (1)–(3). From Eq. (5) and also Eqs. (1)–(3), the deflection of any soil column, where other piles are located in the group around the source pile, can be calculated by Eq. (20) (Fig. 3(a)).

$$\tilde{w}^s \Big|_{r=s} = \tilde{w}^{(1)} \Big|_{r=s} \Omega^{1,2} \tag{20}$$

where \tilde{w}^s is the displacement of the soil column at a radial distance s from the loaded pile, \tilde{w}^1 is the deflection of the source pile, $\Omega^{1,2}$ is the attenuation factor, which is a function of u_r and u_θ . Unlike BWF methods that give only the pile deflection but not the displacement field around the pile, the present method calculates the attenuation factor directly from the single-pile solution, and it does not require another assumption to find the displacement around the pile. The attenuation function can be given as:

$$\Omega^{1,2} = \sqrt{\left\{ \phi_r^2 \cos^2(\theta_{12}) + \phi_\theta^2 \sin^2(\theta_{12}) \right\} \Big|_{r=s}} \tag{21}$$

where θ_{12} is the angle between the radial axes of two piles as shown in Fig. 2.

The displacement field in the soil generated by the source pile can be now obtained on all the nodes in a mesh around the

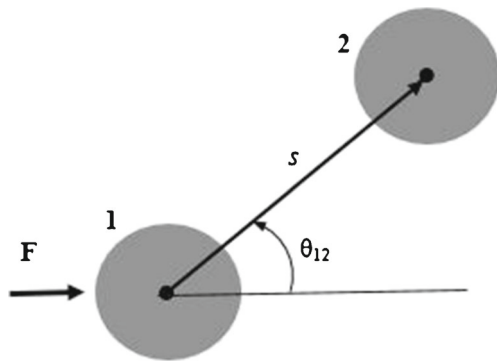


Fig. 2 The radial distance and angle between two piles

pile (Fig. 1). However, the receiver pile will have a different displacement profile than the soil displacement since it has a higher stiffness than the soil layer. The displacement profile of soil at the exact location of the second pile is multiplied by the stiffness of the soil and considered as the continuous force acting along the pile shaft of the receiving pile (Fig. 3). The governing differential equation of a single-pile deflection can be modified to include this effect as presented in Eq. (22). If

the receiver pile is now assumed to present in the neighborhood of the source pile, mathematically, the deflection of the receiver pile can be obtained by solving Eq. (23):

$$\frac{\partial^4 \tilde{w}^{(2)}}{\partial z^4} - 2\tilde{t}^{(2)} \frac{\partial^2 \{ \tilde{w}^{(2)} - \tilde{w}^s \}}{\partial z^2} + \tilde{k}^{(2)} \{ \tilde{w}^{(2)} - \tilde{w}^s \} = 0 \quad (22)$$

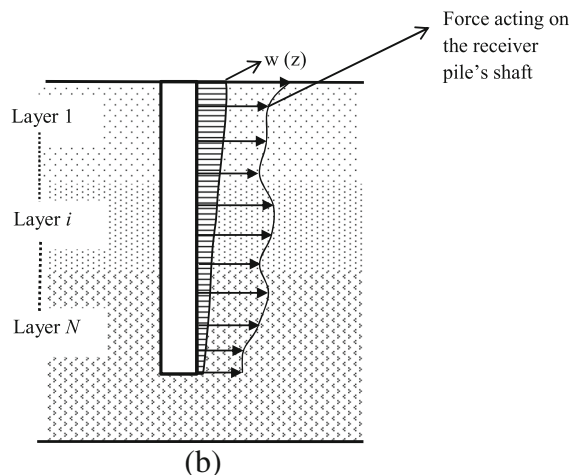
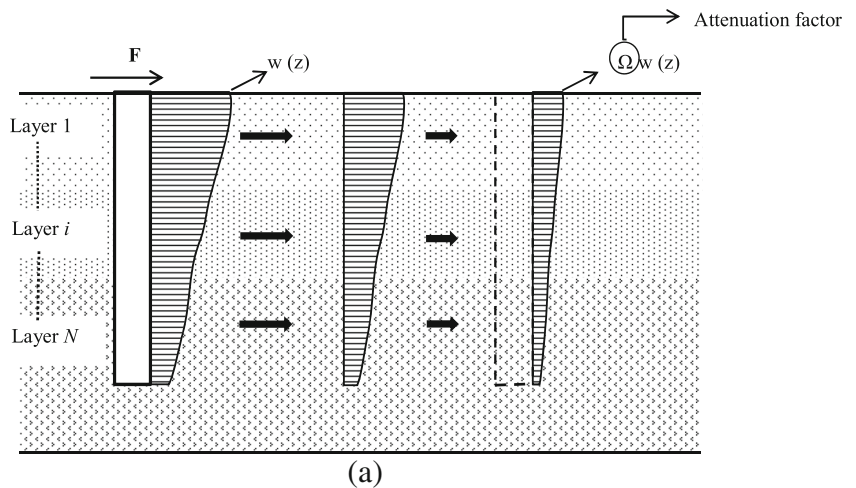
$$\frac{\partial^4 \tilde{w}^{(2)}}{\partial z^4} - 2\tilde{t}^{(2)} \frac{\partial^2 \tilde{w}^{(2)}}{\partial z^2} + \tilde{k}^{(2)} \tilde{w}^{(2)} = -2\tilde{t}^{(2)} \frac{\partial^2 \tilde{w}^s}{\partial z^2} + \tilde{k}^{(2)} \tilde{w}^s \quad (23)$$

$\tilde{w}^{(2)}$ is the deflection of the receiver pile. The right-hand side of Eq. (23) denotes the force acting on the receiver pile. If we define the right-hand side of Eq. (23) as:

$$P(z) = -2\tilde{t}^{(2)} \frac{\partial^2 \tilde{w}^s}{\partial z^2} + \tilde{k}^{(2)} \tilde{w}^s \quad (24)$$

where $\tilde{t}^{(2)}$ and $\tilde{k}^{(2)}$ are the soil parameters for the second pile. The terms in $P(z)$ can be expanded as:

Fig. 3 Pile-soil-pile interaction between two closely spaced piles



$$\begin{aligned}
 -2\tilde{t}^{(2)} \frac{\partial^2 \tilde{w}^{(s)}}{\partial \tilde{z}^2} &= \sinh p\tilde{z} \cos q\tilde{z} \left[-2\tilde{t}^{(2)} \{C_1 p^2 - C_1 q^2 + 2C_3 qp\} \Omega^{(1,2)} \right] \\
 &+ \cosh p\tilde{z} \cos q\tilde{z} \left[-2\tilde{t}^{(2)} \{C_2 p^2 - C_2 q^2 + 2C_4 qp\} \Omega^{(1,2)} \right] \\
 &+ \cosh p\tilde{z} \sin q\tilde{z} \left[-2\tilde{t}^{(2)} \{-C_3 q^2 - C_1 qp + 2C_3 q^2\} \Omega^{(1,2)} \right] \\
 &+ \cosh p\tilde{z} \sin q\tilde{z} \left[-2\tilde{t}^{(2)} \{-C_4 q^2 - C_2 qp + 2C_4 p^2\} \Omega^{(1,2)} \right]
 \end{aligned}
 \tag{25}$$

and

$$\begin{aligned}
 \tilde{k}^{(2)} \tilde{w}^s &= \sinh p\tilde{z} \cos q\tilde{z} (\tilde{k}^{(2)} C_1 \Omega^{(1,2)}) + \cosh p\tilde{z} \cos q\tilde{z} (\tilde{k}^{(2)} C_2 \Omega^{(1,2)}) \\
 &+ \cosh p\tilde{z} \sin q\tilde{z} (\tilde{k}^{(2)} C_3 \Omega^{(1,2)}) + \sinh p\tilde{z} \sin q\tilde{z} (\tilde{k}^{(2)} C_4 \Omega^{(1,2)})
 \end{aligned}
 \tag{26}$$

Then, $P(z)$ can now be put in the form of:

$$\begin{aligned}
 P(z) &= A \sinh p\tilde{z} \cos q\tilde{z} + B \cosh p\tilde{z} \cos q\tilde{z} + C \cosh p\tilde{z} \sin q\tilde{z} \\
 &+ D \sinh p\tilde{z} \sin q\tilde{z}
 \end{aligned}
 \tag{27}$$

where A, B, C, and D are given as:

$$A = \tilde{k}^{(2)} C_1 \Omega^{(1,2)} - 2\tilde{t}^{(2)} \{C_1 p^2 - C_1 q^2 + 2C_3 qp\} \Omega^{(1,2)}
 \tag{28}$$

$$B = \tilde{k}^{(2)} C_2 \Omega^{(1,2)} - 2\tilde{t}^{(2)} \{C_2 p^2 - C_2 q^2 + 2C_4 qp\} \Omega^{(1,2)}
 \tag{29}$$

$$C = \tilde{k}^{(2)} C_3 \Omega^{(1,2)} - 2\tilde{t}^{(2)} \{-C_3 q^2 - C_1 qp + 2C_3 q^2\} \Omega^{(1,2)}
 \tag{30}$$

$$D = \tilde{k}^{(2)} C_4 \Omega^{(1,2)} - 2\tilde{t}^{(2)} \{-C_4 q^2 - C_2 qp + 2C_4 p^2\} \Omega^{(1,2)}
 \tag{31}$$

The differential equation for the deflection of the receiver pile will be in the form of:

$$\frac{\partial^4 \tilde{w}^{(2)}}{\partial \tilde{z}^4} - 2\tilde{t}^{(2)} \frac{\partial^2 \tilde{w}^{(2)}}{\partial \tilde{z}^2} + \tilde{k}^{(2)} \tilde{w}^{(2)} = P(z)
 \tag{32}$$

The solution of Eq. (32) gives us the deflection of the receiver pile. The total solution is equal to the summation of the homogeneous solution and particular solution. Since the right-hand side of Eq. (32) is completely defined, the particular solution of this fourth-order differential equation can be determined analytically. The closed form of this solution can be given as:

$$\tilde{w}^{(2)} = \tilde{w}_t^{(2)} = \tilde{w}_h^{(2)} + \tilde{w}_p^{(2)}
 \tag{33}$$

where $\tilde{w}_h^{(2)}$ will have the same form with the solution of Eq. (5) with different constants, and $\tilde{w}_p^{(2)}$ can be expressed as:

$$\tilde{w}_p^{(2)} = \Gamma_1 \Psi_1 + \Gamma_2 \Psi_2 + \Gamma_3 \Psi_3 + \Gamma_4 \Psi_4
 \tag{34}$$

where

$$\Psi_1 = \sinh p\tilde{z} \cos q\tilde{z}
 \tag{35}$$

$$\Psi_2 = \cosh p\tilde{z} \cos q\tilde{z}
 \tag{36}$$

$$\Psi_3 = \cosh p\tilde{z} \sin q\tilde{z}
 \tag{37}$$

$$\Psi_4 = \sinh p\tilde{z} \sin q\tilde{z}
 \tag{38}$$

and where Γ_j is defined as:

$$\Gamma_1 = \frac{\{A\alpha + D\beta\}}{K}
 \tag{39}$$

$$\Gamma_2 = \frac{\{B\alpha + E\beta\}}{K}
 \tag{40}$$

$$\Gamma_3 = \frac{D\alpha - A\beta}{K}
 \tag{41}$$

$$\Gamma_4 = \frac{E\alpha - B\beta}{K}
 \tag{42}$$

Also, α , β , and K are defined respectively as:

$$\alpha = p^4 + q^4 - 6p^2 q^2 - 2(p^2 - q^2)(a^2 - b^2) + (a^2 + b^2)^2
 \tag{43}$$

$$\beta = 4p^2 q^2 (q^2 - p^2 + a^2 - b^2)
 \tag{44}$$

$$\begin{aligned}
 K &= \left((a+p)^2 + (b+q)^2 \right) \left((a-p)^2 + (b+q)^2 \right) \\
 &\left((a+p)^2 + (b-q)^2 \right) \left((a-p)^2 + (b-q)^2 \right)
 \end{aligned}
 \tag{45}$$

where

$$a = \sqrt{\frac{\sqrt{\tilde{k}^{(2)}} + \tilde{t}^{(2)}}{2}}
 \tag{46}$$

$$b = \sqrt{\frac{\sqrt{\tilde{k}^{(2)}} - \tilde{t}^{(2)}}{2}}
 \tag{47}$$

Note that the definitions of the normalized slope $\tilde{\Theta}^{(2)}$, normalized moment $\tilde{M}^{(2)}$, and normalized shear force $\tilde{S}^{(2)}$ along the second pile are derived from the definition of deflection by taking derivatives with respect to \tilde{z} . Therefore, the rotation, moment, and shear force equations can be determined for the second pile as follows:

$$\tilde{\Theta}^{(2)} = \frac{d\tilde{w}^{(2)}}{d\tilde{z}}
 \tag{48}$$

$$\tilde{M}^{(2)} = \frac{d\left(\tilde{w}^{(2)}\right)^2}{d\tilde{z}^2}
 \tag{49}$$

$$\tilde{S}^{(2)} = \frac{d\left(\tilde{w}^{(2)}\right)^3}{d\tilde{z}^3} - 2\tilde{k} \frac{d\left(\tilde{w}^{(2)}\right)^2}{d\tilde{z}^2} \tag{50}$$

Equations (48)–(50) are, respectively, given analytically in the open form as:

$$\tilde{\Theta}^{(2)} = C_1(a\Phi_2 - b\Phi_4) + C_2(a\Phi_1 - b\Phi_3) + C_3(a\Phi_4 - b\Phi_2) + C_4(a\Phi_3 - b\Phi_1) + \Gamma_1(p\Psi_2 - q\Psi_4) + \Gamma_2(p\Psi_1 - q\Psi_3) + \Gamma_3(p\Psi_4 + q\Psi_2) + \Gamma_4(p\Psi_3 + q\Psi_1) \tag{51}$$

$$\begin{aligned} \tilde{M}^{(2)} = & C_1\left[\left((a)^2 - (b)^2\right)\Phi_1 - 2ab\Phi_3\right] + C_2\left[\left((a)^2 - (b)^2\right)\Phi_2 - 2ab\Phi_4\right] \\ & + C_3\left[\left((a)^2 - (b)^2\right)\Phi_3 + 2ab\Phi_1\right] + C_4\left[\left((a)^2 - (b)^2\right)\Phi_4 + 2ab\Phi_2\right] \\ & + \Gamma_1\left[(p^2 - q^2)\Psi_1 - 2pq\Psi_3\right] + \Gamma_2\left[(p^2 - q^2)\Psi_2 - 2pq\Psi_4\right] \\ & + \Gamma_3\left[(p^2 - q^2)\Psi_3 + 2pq\Psi_1\right] + \Gamma_4\left[(p^2 - q^2)\Psi_4 + 2pq\Psi_2\right] \end{aligned} \tag{52}$$

$$\begin{aligned} \tilde{S}^{(2)} = & C_1\left[a\left((a)^2 - 3(b)^2\right)\Phi_2 + b\left((b)^2 - 3(a)^2\right)\Phi_4\right] \\ & + C_2\left[a\left((a)^2 - 3(b)^2\right)\Phi_1 + b\left((b)^2 - 3(a)^2\right)\Phi_3\right] \\ & + C_3\left[a\left((a)^2 - 3(b)^2\right)\Phi_4 + b\left((b)^2 - 3(a)^2\right)\Phi_2\right] \\ & + C_4\left[a\left((a)^2 - 3(b)^2\right)\Phi_3 + b\left((b)^2 - 3(a)^2\right)\Phi_1\right] \\ & - 2\tilde{t}^{(2)}\left[C_1(a\Phi_2 - b\Phi_4) + C_2(a\Phi_1 - b\Phi_3) + C_3(a\Phi_4 + b\Phi_2) + C_4(a\Phi_3 + b\Phi_1)\right] \\ & + \Gamma_1(p(p^2 - 3q^2)\Psi_2 + q(q^2 - 3p^2)\Psi_4) \\ & + \Gamma_2(p(p^2 - 3q^2)\Psi_1 + q(q^2 - 3p^2)\Psi_3) \\ & + \Gamma_3(p(p^2 - 3q^2)\Psi_4 - q(q^2 - 3p^2)\Psi_2) \\ & + \Gamma_4(p(p^2 - 3q^2)\Psi_3 - q(q^2 - 3p^2)\Psi_1) \\ & - 2\tilde{t}^{(2)}\left[\Gamma_1(p\Psi_2 - q\Psi_4) + \Gamma_2(p\Psi_1 - q\Psi_3) + \Gamma_3(p\Psi_4 + q\Psi_2) + \Gamma_4(p\Psi_3 + q\Psi_1)\right] \end{aligned} \tag{53}$$

Equations (33) and (51)–(53) are the total solutions for $\tilde{w}^{(2)}$, $\tilde{\Theta}^{(2)}$, $\tilde{M}^{(2)}$, and $\tilde{S}^{(2)}$, respectively, which are the summations of particular and homogeneous solutions. This section summarized the solution method for two piles, one of which is loaded, to determine the deflection of the unloaded pile under the interaction effect. This pile-soil-pile interaction can be generalized for multiple piles when all the piles are loaded with the same or different loads. The effect of each pile on the other piles can be determined and the total deflections of piles accounting for the group effect can be obtained. A flow chart describing the application of the algorithm to pile groups is given in Fig. 4. These algorithm steps are necessary to obtain the consistent deflections and soil parameters after the interaction forces acted on the piles. This method takes the superposition approach as a basis when calculating total interaction in a group, however, it also looks for the consistent γ_i values, rather than simply adding up the

interaction forces, during the individual analysis of piles. The definitions of γ_i values include the deflection of the pile being analyzed; therefore, they need to be updated after interaction forces are taken into account. When extending the solution to larger pile groups consisting of more than two piles, the solution obtained from a single-pile analysis is used to calculate the interaction forces acting on other piles in the group. Assuming all the piles are in identical conditions, this single-pile solution is accepted to be the solution of one of the piles and attenuation factors as well as interaction forces on other piles are determined. The attenuation factors and interaction forces received by piles will vary depending on their respective locations. After total forces on the piles are calculated, an iteration on γ_i values starts and continues until the desired accuracy in between two consequent steps is acquired. Then, the procedure can be repeated for the rest of the piles. At this point, another global iterative scheme might be added to check the differences in γ_i values for each pile again after all the interaction forces and updated displacement values are determined. However, the current algorithm works well under the linear elastic material assumption. The next section presents the application of the proposed method to example problems.

Numerical examples

The numerical examples require the domain to be discretized as shown in Fig. 1. Three hundred and fifty-one increments in circumferential direction which give $\Delta\theta = 360^\circ/351 \approx 1.02^\circ$ have been chosen. There are 351 nodes in radial direction with $\Delta r = 0.05$ m, which reaches a total radial distance of 17.55 m from the pile center, and also 101 nodes for each layer along the pile length.

Radial nodes are used to determine $\phi_r(r)$ and $\phi_\theta(r)$ over the soil domain surrounding a pile. These functions simply indicate how far the displacement of the soil around a pile would extend from that pile. Thus, one number to cover the largest domain, which is the diagonal distance in Example 3, was selected for the number of radial nodes. In Example 3, the biggest distance is between the most distant corner piles and it is less than 17 m. For the example problems, more radial nodes were also used and it was found that the results were not changed significantly; therefore, only the results with 351 radial nodes were reported. The number of nodes in the vertical direction is basically needed to determine the deflection profile of the pile and surrounding soil. Also, the interaction forces are calculated by using these nodes along the pile length. Hence, the number of nodes in the vertical direction mostly depends on how smooth force or deflection profile is needed. As a result, this grid has been found sufficient to acquire the accuracy in the comparisons given in this section.

Example 1: interaction effect

The first example considers two identical piles, each of which has a length of 10 m and a radius of 0.6 m. The piles are fixed at the bottom and the source pile is loaded by a force of 600 kN on top, while the receiver pile is not loaded. Elasticity moduli have been taken for the pile and soil, respectively, as $E_p = 28 \times 10^9$ kPa and $E_s = 7 \times 10^6$ kPa for the piles and soil, respectively. This example demonstrates the effect of a laterally loaded pile on the displacement profile of an unloaded pile; therefore, the displacement of the receiver pile will be due to the interaction effect solely (Fig. 5).

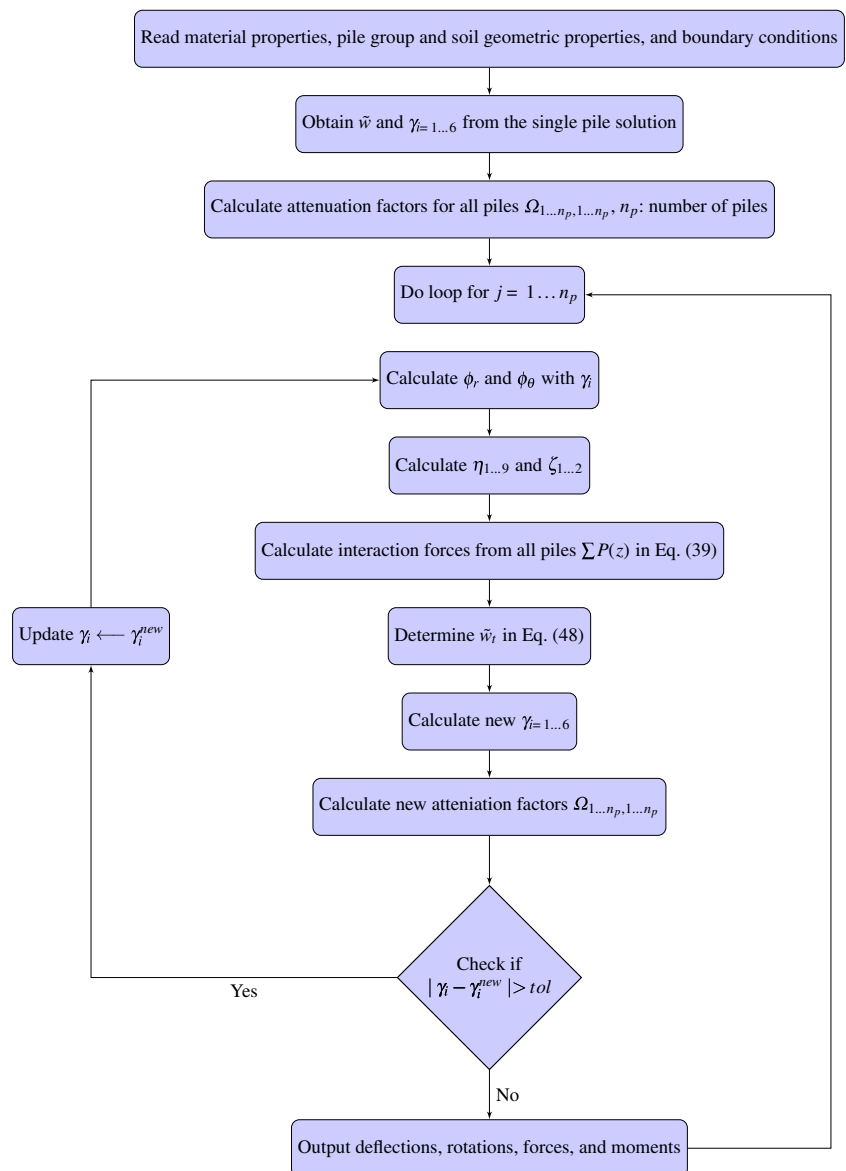
Example 2: small pile groups

The next example presents the application of the proposed approach to the small pile groups consisting of two, four, and six piles.

Two-pile group

For the first case which is a two-pile group, the material properties and geometry are the same as in Example 1. The pile spacing s , radial distance, between the piles is 4 m, and all the piles have the same load, which is 600 kN. The pile group consisting of two piles investigates two different pile line-ups:

Fig. 4 Flow chart of the solution algorithm



(i) piles in line and (ii) piles side by side. To investigate the accuracy of the proposed method, the results of the present analysis are compared with those of the finite element method.

Four- and six-pile group

The next case includes the application of the method to the pile groups consisting of four piles and six piles, respectively. Figure 8 presents the pile placing for four- and six-pile groups. For this example, the pile diameters have been chosen to be 1 m. The rest of the problem geometry as well as material properties are the same as described in Example 1. The main purpose of this example is to demonstrate the robustness of the proposed approach. The comparisons of the results with the finite element (FE) model results are provided, and also analysis times for two-pile, four-pile, and six-pile groups and also the FEM analysis times are compared.

Example 3: pile group with a cap

Piles in a group generally work under a rigid cap. This example analyzes a group of nine piles, which are connected to each other by a rigid pile cap on top. This kind of group will, in essence, contain a similar load transfer mechanism; therefore, it entails the necessity for seeing load distribution among the piles in the group. The loading direction and pile numbering for this example are as shown in Fig. 11(a). The piles are placed symmetrically about the origin of $x-y$ plane with $s = 6$ m, $r_p = 0.5$ m, and $L_p = 6$ m. The pile cap imposes a boundary condition, which dictates a fixed rotation at top $\tilde{\theta} = 0$ and the rigid cap displacement u_{top} of 10 mm for all the piles in the group. Other material parameters are $E_p = 25 \times 10^{10}$ Pa, $\nu = 0.2$, and $E_s = 10 \times 10^7$ Pa. As opposed to the previous examples, the free bottom-end boundary condition is

assumed, which will result in a base displacement for the piles (Fig. 11(b)).

Example 4: group efficiency

This example intends to provide a comparison of the present study with the previous work by Salgado et al. (2014) available in the literature. Group efficiency charts are convenient to compare the average load taken by each pile in pile groups with that of a single pile under identical conditions (Salgado et al. 2014). A group efficiency chart obtained from the response of the pile group considered in Example 3 in a two-layered soil is presented. The soil layers have the same thickness ($H_1 = H_2$) and plots are provided with different E_{s1}/E_{s2} ratios where E_{s1} and E_{s2} are Young's moduli, respectively, for the upper layer and lower layer as shown in Fig. 13(a). Group efficiency, the ratio of average force on each pile to the single-pile force, is defined by

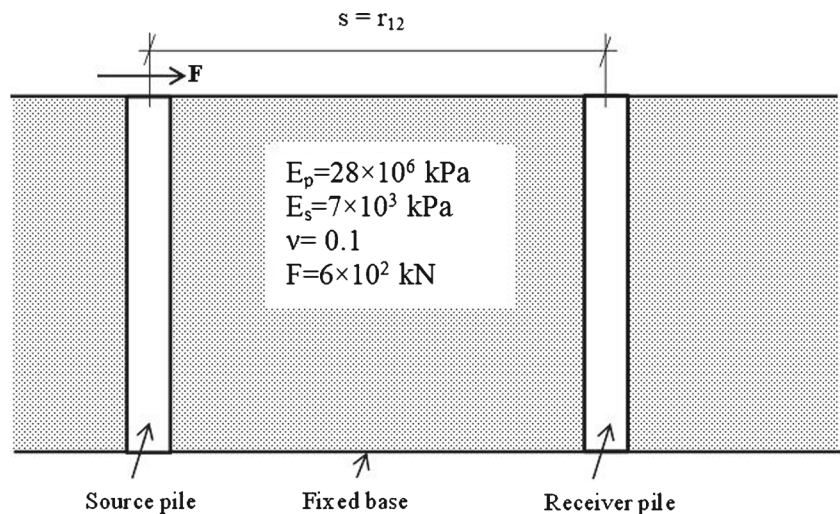
$$\eta = \frac{(F_T/n_p)}{F_s} \tag{54}$$

where F_T is the summation of forces on the piles, n_p is the total number of piles, and F_s is the top force of a single pile caused by the same cap displacement given in Example 3. For a slightly different case with $E_p = 25 \times 10^9$ Pa and $E_{s1} = E_{s2} = 10 \times 10^6$ Pa, the group efficiency comparison with Salgado et al. (2014) is presented in Fig. 14.

Results and discussion

The set-up given in Example 1 reveals how the shadowing effect between closely spaced two piles causes significant interaction displacements experienced by the receiver pile. The deflection profiles of the receiver pile with varying Poisson's

Fig. 5 Problem geometry and material properties for Example 1 to demonstrate the load transfer from a source (loaded) pile to a receiver pile



ratios ν and pile spacings s are given in Fig. 6. The comparisons of the displacements of the source and receiver piles are also presented in Fig. 6. Figure 6(a) presents the effect of material properties in terms of Poisson ratio of the soil layer on the receiver pile deflections. As it is seen from Fig. 6, the higher Poisson's ratio, the larger deflections, which is expected. Figure 6(b) presents the significant effect of the radial distance on the additional pile deflections, and Fig. 6(c) compares the deflection of the source pile with that of the receiver pile when $s = 4$ m. Both figures present the considerable interaction effect.

Figure 7 shows the pile deflections and comparisons with the FEM results. In Fig. 7, the two cases were considered, which are piles placed in line and piles placed side by side. These two different placements of the piles have been chosen to simply show the shadowing effect on piles depending on their locations. Piles are exposed to more shadowing effects when they are placed as in Fig. 7(a) since the second pile is in the loading direction. The example was set-up to check if the model is capable of capturing this behavior. The comparisons presented consistent results with those of the FEM analyses for both cases in which the loading directions are different. As

Fig. 6 The interaction effect on the receiver pile. **a** The deflection profile of the receiver pile varying with different Poisson's ratio when $s = 4$ m. **b** The deflection profile of the receiver pile varying with pile spacing. **c** Comparison of receiver pile's deflection with the source pile deflection

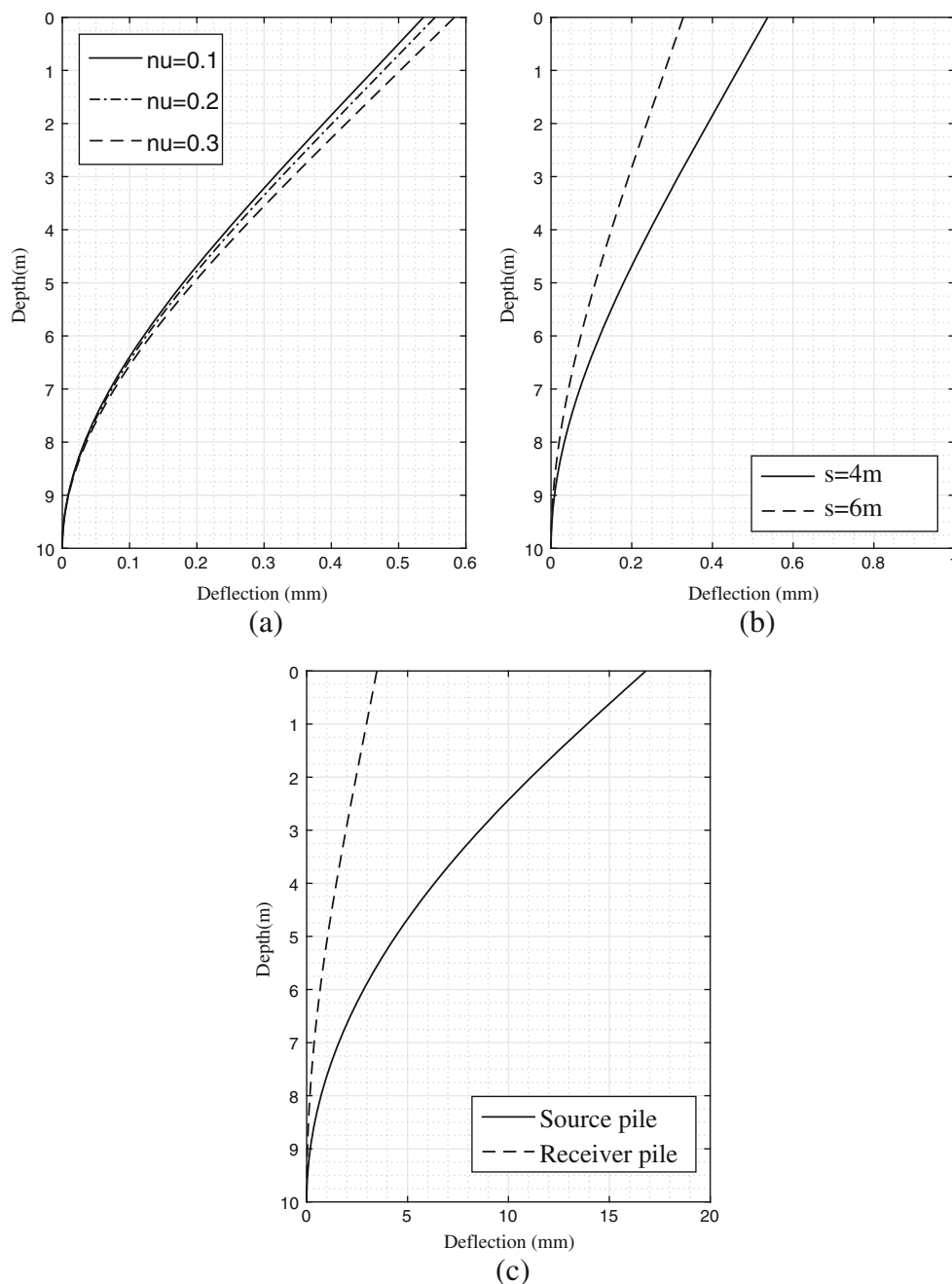
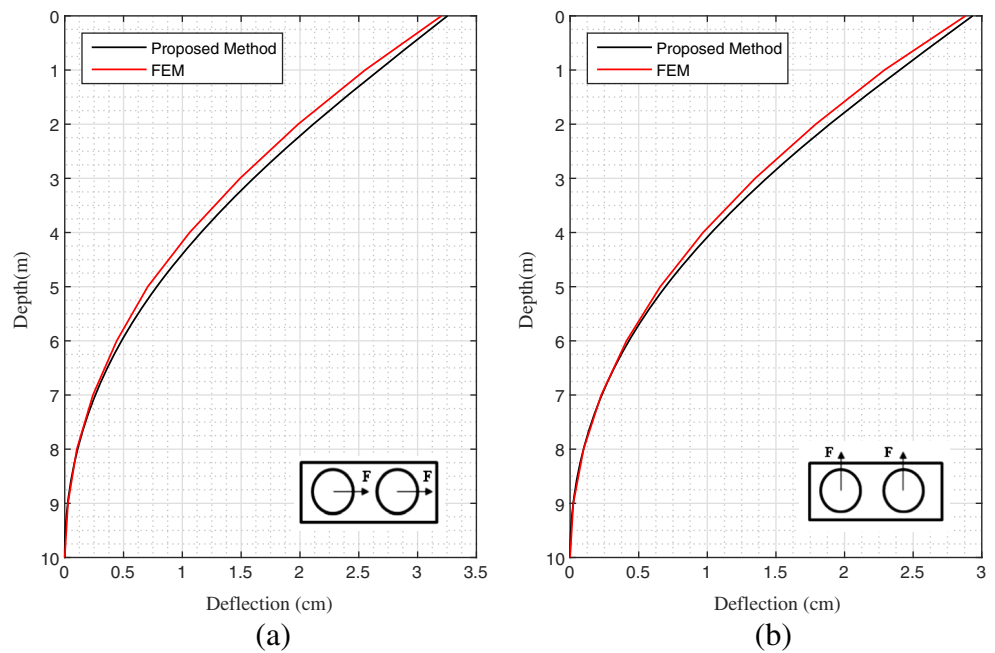


Fig. 7 Comparison of the results with the finite element model results **a** two piles placed in line, **b** two piles placed side by side. The deflection curves of the piles in both line-ups are the same due to symmetry



expected, the model worked well and gave less displacements for piles which are placed side by side as in Fig 7(b).

Figure 8 shows the formations of the four- and six-pile groups. Figure 9(a) presents the deflection of a pile in the four-pile group since the deflection profiles of the other piles in the group are the same due to the symmetry in the geometry and loads. Figure 9(b) and (c) show the deflections of pile-1, which is the mid-front row pile, and pile-2, which is the front left corner pile, respectively, for the six-pile group. Figure 9 also includes the FEM results and the deflection profile of an identical single pile. The single-pile deflection is given to emphasize the importance of the shadowing effect as the number of piles placed in the close vicinity increases.

As clearly seen in Fig. 9(a), the model results capture the pile deflections obtained from the finite element model in the four-pile group. All the piles in this group have the identical deflection profile as expected and the results of the model are in accordance with the FEM results. Figures 9(b) and (c) show that pile-1 has larger displacements. The reason is that this pile

is surrounded by other piles at the symmetry line and exposed to the load transfers from both sides. Thus, the interaction effect for this pile is the largest among all. The deflection of a separate identical single pile under the same load in Fig. 9 indicates the substantial group effect in pile groups.

Moreover, Table 1 compares the analysis times for two-pile (in-line), four-pile, and six-pile groups and those of the FEM analyses. It shows the computational efficiency and supports the proposed method for possible applicability to large-scale pile groups. Biased meshes as seen in Fig. 10 were used in the FE analyses to better capture maximum displacements. The grid of mesh used in the present analyses has 351 radial nodes, 351 circumferential increments, and 100 nodes in vertical directions. It is apparently denser than the finite element mesh given in Table 1 and also shown in Fig. 10, which also proves the robustness of the method; one reason is that the analytical solution of the pile deflection accounting for the group effect has been obtained and implemented. Unlike the finite element method, the proposed approach uses this analytical solution to

Fig. 8 Small pile groups of identical piles showing pile placement for **a** four-pile group, **b** six-pile group

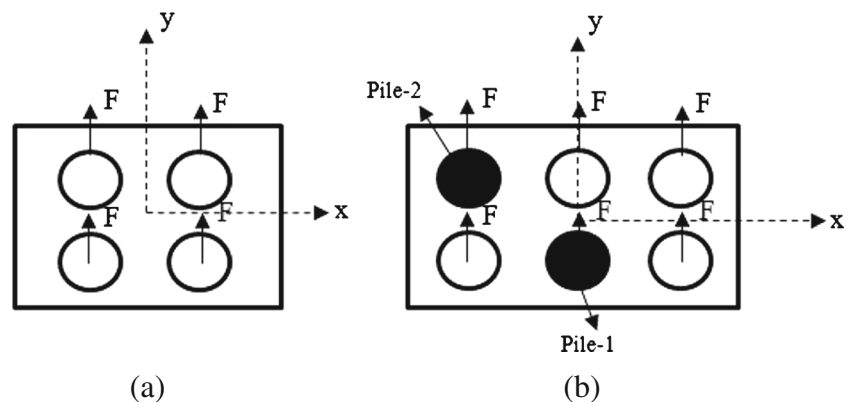
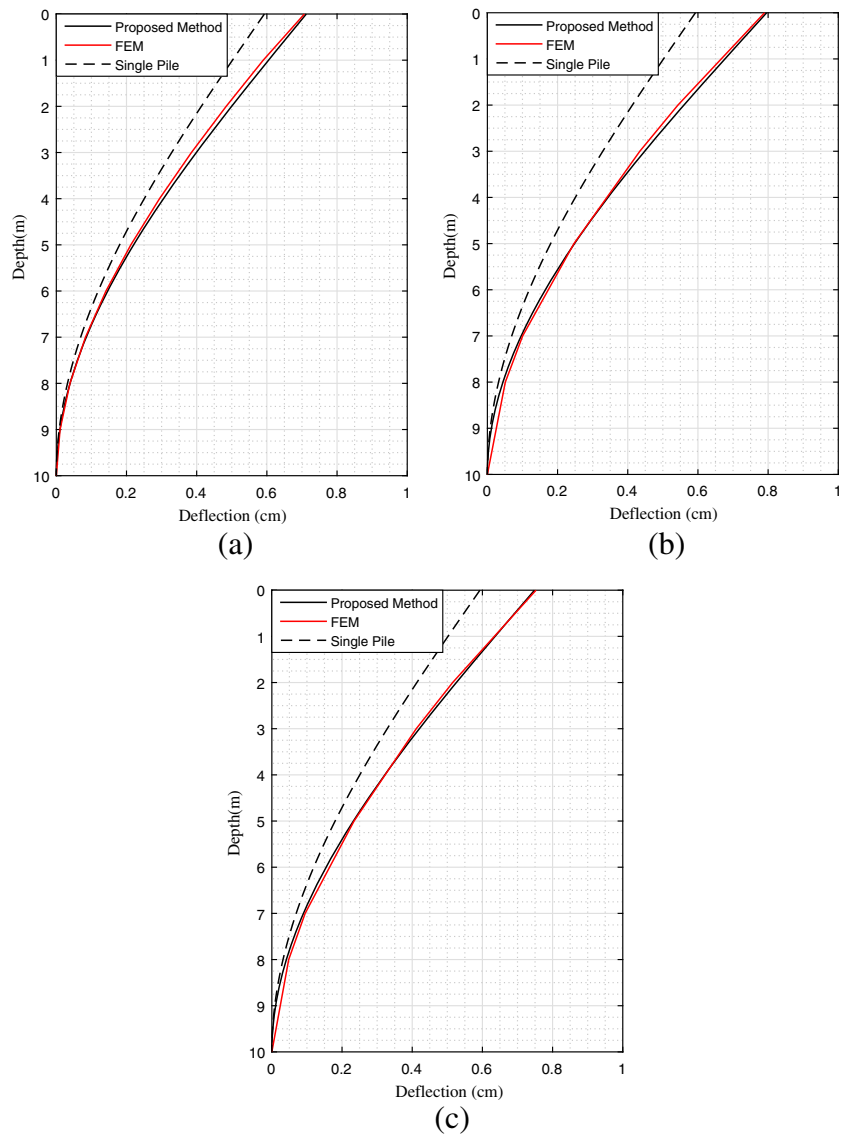


Fig. 9 Comparison of the analysis results of the proposed method with the finite element model results for pile groups **a** identical deflection profile of each pile in the four-pile group, **b** the deflection profile of the mid-column pile (pile-1) in the six-pile group, **c** the deflection profile of the front corner pile (pile-2) in the six-pile group



obtain the pile deflection; however, it calculates the soil parameters and displacements descending with radial distance in a numerical way. This performance is very important, especially when it is compared to the commercial FEM software which requires a significant amount of time in pre-/post-processing and also expertise.

Although the soil stiffness parameters k and t take the stiffness of the soil around the pile, this approach does not consider the existence of the other piles directly while calculating the response of individual piles. The present method ignores the additional stiffness increase in soil layers, which is taken into account by FEM clearly, due to the existence of the other

Table 1 Analysis times of the proposed method and finite element method for each case in Example 2. The present method used 351 radial nodes, 351 circumferential increments, and 100 nodes in vertical directions for the analyses

Case name	Model analysis time (sec)	FE analysis time (sec)	Number of nodes in FE analysis
Group of 2 piles in line	0.67187	13.06	3495
Group of 4 piles	1.25000	13.56	5190
Group of 6 piles	1.64063	15.93	11,784

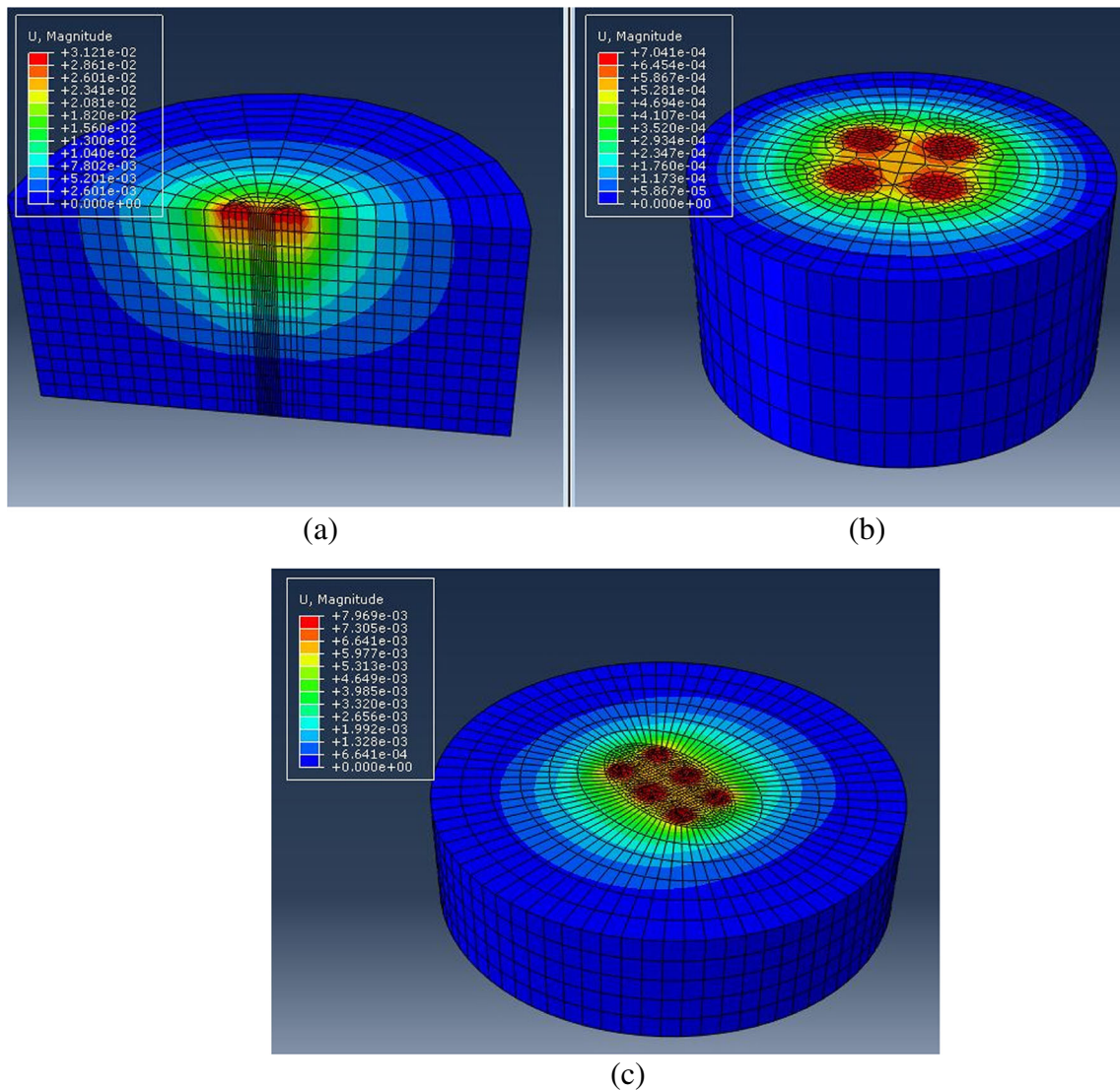
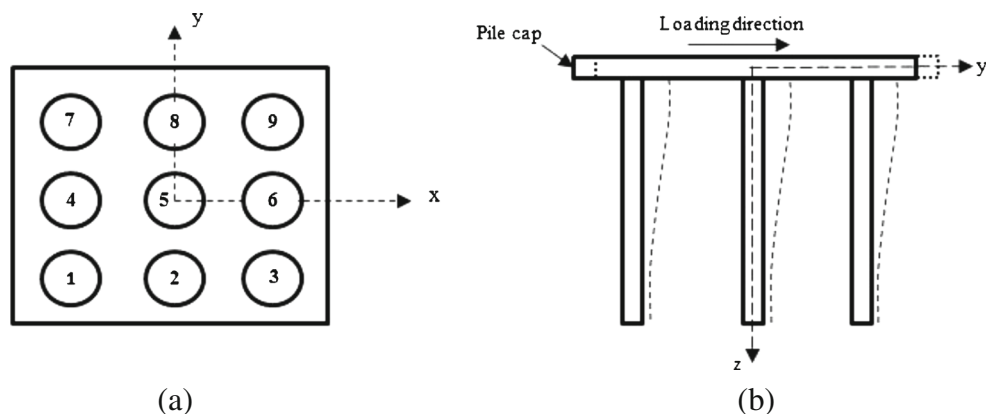


Fig. 10 Finite element meshes for the pile groups **a** two piles (half domain), **b** four piles, and **c** six piles

piles in the physical problem when calculating the deflection of piles. Even though the proposed method can be developed to take such stiffness increase by assigning the elastic material properties of the pile into the soil

column in the mesh, this assumption is alleviated by the iterative algorithm to have consistent pile deflections and the comparisons (Figs. 7 and 9) with the FEM results basically prove that it does not have a significant effect on the

Fig. 11 Pile group with a cap. **a** Top view of the pile group, **b** schematic side view



response with the linear elastic material assumption for soil and pile (Fig. 11).

Figure 11(a) and (b) show the pile numbering and schematic side view of the nine-pile group, respectively. Figure 12 summarizes the analysis results for the problem described in Example 3. The pile cap imposes the same top displacement for the piles in this example. Figures 12(a), (b), and (c) present the deflection, shear force, and moment, respectively, along the pile lengths in the group. The plots are presented only for piles 4, 5, 7, and 8 since other piles will have the same response with these piles depending on their location due to the symmetry in the $x-y$ plane. Figure 12 also indicates a strong interaction effect again as observed in the previous examples. The free-end displacement for pile-5 is larger than the other piles since it is located in the symmetry center and exposed to the highest total interaction force. The top force and moments of the piles are all smaller

than that of a single pile. The results in Fig. 12(b) and (c) indicate that the corner piles are exposed to more top force and top moment compared to the interior piles when there is a rigid pile cap.

For pile groups, Eqs. (12), (13), (16), and (17) should be given careful attention, especially in the case of closely spaced pile groups. If piles loaded by large head forces are placed in close vicinity of the other piles, mathematically, this model can estimate interaction forces causing large pile head deflections. This additional interaction deflection would enforce the pile to have a larger pile head force based on Eq. (12), but it will be constrained by the imposed force BC at the top. A similar mechanism can be possible for the other top BC case, in which a prescribed displacement representing a rigid pile-cap is applied as the top BC, although the pile-head force is determined after interaction effects are taken into account by applying Eq. (50). For both cases, it would be needed to

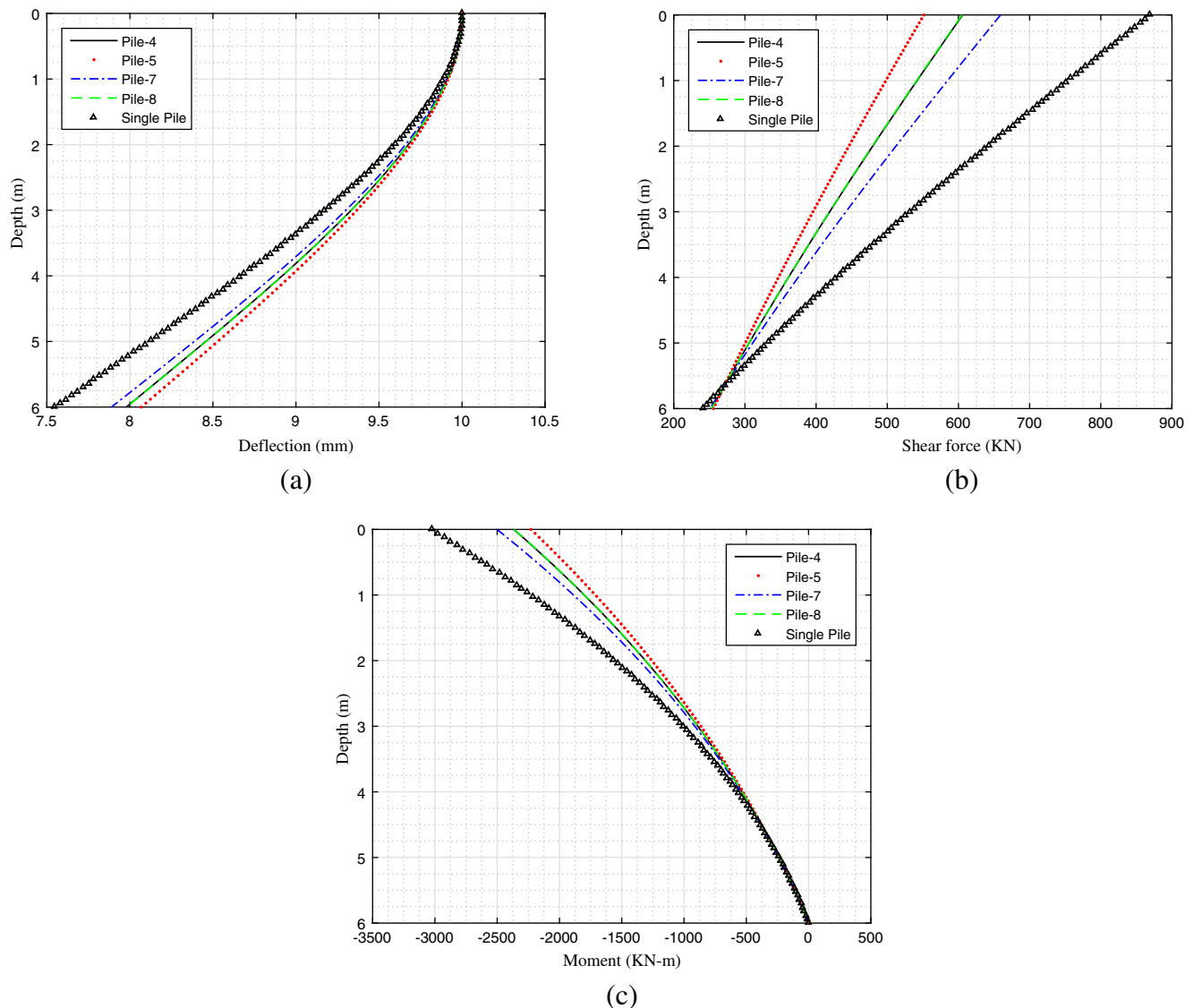


Fig. 12 Nine-pile group with a rigid cap **a** deflection, **b** shear force, and **c** moment diagrams along the pile lengths

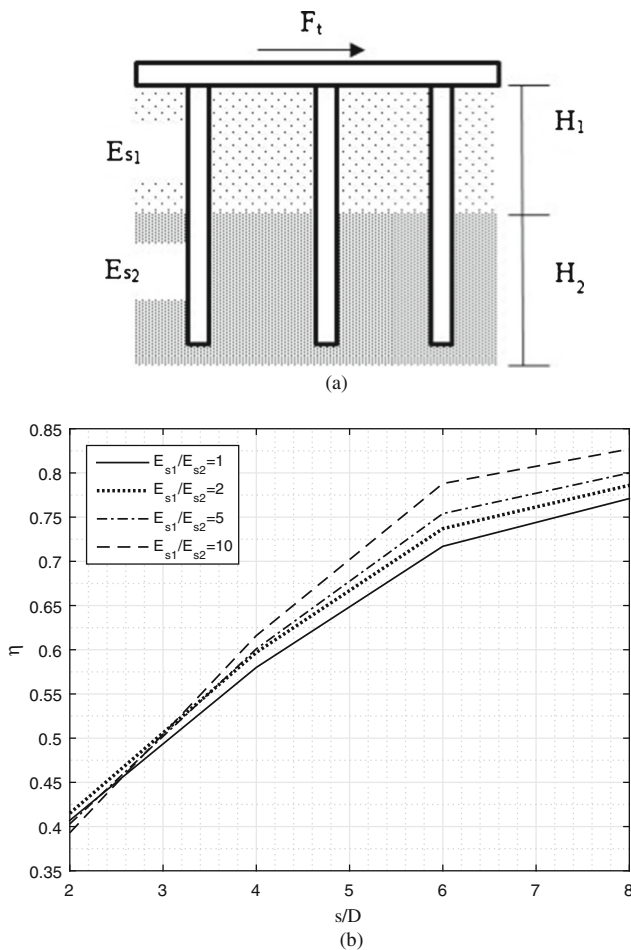


Fig. 13 Group efficiency in a single-layered soil and two-layered soils with various E_{s1}/E_{s2} ratios

implement a constraint which prevents the mathematical solution from creating extraordinary interaction forces on the other piles. As yet, such large interaction forces have not been

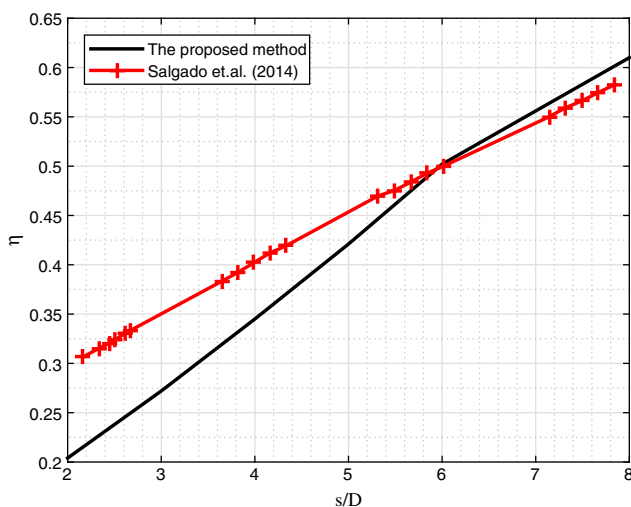


Fig. 14 Comparisons of the results with Salgado et al. (2014) for the same geometry and properties for a group embedded in a single layer

observed in the numerical examples. It can be seen that the method works well as the FE analysis results present a very close match for pile deflections for the applied force BC. In addition, the body deflections did not go beyond the pile head deflections due to interaction forces for the problem considered in Example 3 as seen in Fig. 12. For a same prescribed displacement value, piles in a group will have less head forces—the total load is shared among piles—compared to a single pile as mentioned above, but this force value will vary for piles because of their locations in the group. By applying this approach, the displacement-force curve of a pile group with a rigid pile-cap can be obtained through the summation of the pile head forces which will be equal to the total load applied on the pile group at that particular lateral displacement. In the proposed approach, the governing differential equation of a pile is solved with updated interaction forces acting as a distributed load. The solution satisfies the imposed BCs and interaction forces create only additional pile deflection.

Figure 13(a) shows the pile group described in Example 4. Figure 13(b) presents η vs. s/D ratios to be employed for a variety of different pile geometries and pile spacings for the problem. Figure 13(b) also shows group efficiency η with varying stiffness ratios between the upper layer and lower layer. Figure 13(b) expresses that group efficiency η increases as the pile spacing increases, which indicates the average load on piles also ascends up to a point and the load transfer (interaction forces) decreases. This behavior is magnified when the elasticity modulus of the upper layer modulus gets larger than that of the lower layer. But it loses its influence as it reaches around $s/D = 6$ because the large pile spacing causes each pile to behave like an isolated pile, which might not be desired.

Figure 14 presents a comparison with the previous study by Salgado et al. (2014). Although the methods show a small difference for the range $s/D = 2..6$, the general trend is similar, especially for $s/D = 6..8$. Salgado et al. (2014) indicates higher group efficiency value for the range $s/D = 2..6$, while the proposed method in this study estimates lower values of group efficiency for the same range. Both methods approximate to each other for the higher values of s/D . Salgado et al. (2014) assumed a displacement field which allows the displacements in loading direction only in a Cartesian coordinate system, whereas this study enables the soil to have displacements in both radial and circumferential directions. However, the main source of the difference can be the algorithm and mathematical model used by Salgado et al. (2014) in the determination of the decay function and soil parameters. Researchers also employed a set of simplifications to consider dominant terms when solving the system of coupled equations for the decay functions in the iterative algorithm. Eventually, all these are anticipated to

result in small variations in the comparison of the s/D ratios.

Conclusions

This study proposed a new method for calculating the response of laterally loaded pile groups embedded in layered soils. The analyses for pile groups with different sets of BCs have been presented and the results have been compared to the results of the FEM analyses and a previous study. Based on the results presented in this study, one can conclude that the comparisons of the proposed method with the FEM analyses show matching results and a better performance than the FEM analyses. The results also show a good agreement with the previous work by Salgado et al. (2014) for the group efficiency example. The comparisons of analysis times with the FEM times also present the computational efficiency and robustness of the method. Especially, for large pile groups which can be consisting of tens of piles, modeling efforts such as meshing and convergence analyses may require substantial amount of time, whereas the Fortran code developed for this study only requires a simple input file, which includes mainly geometric, material properties, and load data. Also, it depends on users to decide on the number of radial and vertical points. These computational advantages demonstrate the possibility to further extend the model to include soil plasticity that will provide the opportunity to model experiment results for which deformation range can no longer be modeled by elastic behavior assumptions.

It has been observed that the existence of other piles when calculating the soil stiffness in the single pile response does not affect the group response significantly or mitigated by γ_m iterations. Moreover, determining the attenuation function analytically without any assumptions provides substantially effective and accurate interaction force calculations. These two observations also support that the present method can be a basis for further development for cases, as mentioned above, which demand more computational power. Overall, the model proposed in this study provides the opportunity for researchers to investigate the problem in a computationally efficient way.

The effect of the interaction is also clearly observed in the results. Clear shadowing effects have been obtained in free-head and rigid-cap examples. For the pile groups with rigid-pile cap and free-end conditions, the interaction effects cause more tip displacement for the piles in a group. A group efficiency chart was presented which can be applied to pile group analysis assuming that deformations stay small and elastic behavior assumptions remain valid. The analyses indicated that the piles at the outer corner for this group are exposed to more force than the interior piles. Group efficiency increases with s/D ratio, especially between $s/D = 2..6$, while this ratio gets less efficient after that range. For a soft soil layer

underlying a stiffer layer with the same thickness, this effect is even more highlighted by higher E_{s1}/E_{s2} ratios.

Acknowledgments The author thanks Dr. Rodrigo Salgado for the valuable discussions on the single-pile analysis method.

Funding information The author acknowledges the funding by TUBITAK under Grant BIDEB 2232-116C087.

References

- Abdrabbo F, Gaaver K (2012) Simplified analysis of laterally loaded pile groups. *Alex Eng J* 51(2):121–127
- Ai ZY, Feng DL (2014) Bem analysis of laterally loaded pile groups in multi-layered transversely isotropic soils. *Eng Anal Bound Elem* 44: 143–151
- Ai ZY, Li ZX (2015) Dynamic analysis of a laterally loaded pile in a transversely isotropic multilayered half-space. *Eng Anal Bound Elem* 54:68–75
- Ai ZY, Li ZX, Wang LH (2016) Dynamic response of a laterally loaded fixedhead pile group in a transversely isotropic multilayered half-space. *J Sound Vib* 385:171–183
- Aşık MZ (1999) Dynamic response analysis of the machine foundations on a nonhomogeneous soil layer. *Comput Geotech* 24(2):141–153
- Aşık MZ, Vallabhan C (2001) A simplified model for the analysis of machine foundations on a nonsaturated, elastic and linear soil layer. *Comput Struct* 79(31):2717–2726
- Ashour M, Pilling P, Norris G (2004) Lateral behavior of pile groups in layered soils. *J Geotech Geoenviron* 130(6):580–592
- Bahrami A, Nikraz H (2017) Generalized Winkler support properties for far field modeling of laterally vibrating piles. *Soil Dyn Earthq Eng* 92:684–691
- Banerjee PK, Driscoll RM (1976) Three-dimensional analysis of raked pile groups. *Proc Inst Civ Eng* 61(4):653–671
- Basu D, Salgado R, Prezzi M (2009) A continuum-based model for analysis of laterally loaded piles in layered soils. *Geotechnique* 59(2): 127–140
- Bonakdar L, Oumeraci H (2015) Pile group effect on the wave loading of a slender pile: a small-scale model study. *Ocean Eng* 108:449–461
- Bransby MF (1996) Difference between load-transfer relationships for laterally loaded pile groups: active p - y or passive p -d. *J Geotech Eng* 122(12):1015–1018
- Brown DA, Shie C-F (1991) Some numerical experiments with a three dimensional finite element model of a laterally loaded pile. *Comput Geotech* 12(2):149–162
- Brown DA, Reese LC, O'Neill MW (1987) Cyclic lateral loading of a large-scale pile group. *J Geotech Eng* 113(11):1326–1343
- Comodromos EM, Papadopoulou MC (2013) Explicit extension of the p-y method to pile groups in cohesive soils. *Comput Geotech* 47:28–41
- Comodromos EM, Ptilakis KD (2005) Response evaluation for horizontally loaded fixed-head pile groups using 3-d non-linear analysis. *Int J Numer Anal Methods Geomech* 29(6):597–625
- Duncan JM, Evans LT, Ooi PSK (1994) Lateral load analysis of groups of piles and drilled shafts. *J Geotech Eng* 120(6):1034–1050
- Elhakim AF, Khouly MAAE, Awad R (2016) Three dimensional modeling of laterally loaded pile groups resting in sand. *HBRC J* 12(1): 78–87
- Fan C-C, Long H, J. (2007) A modulus-multiplier approach for non-linear analysis of laterally loaded pile groups. *Int J Numer Anal Methods Geomech* 31(9):1117–1145

- Giannakos S, Gerolymos N, Gazetas G (2012) Cyclic lateral response of piles in dry sand: finite element modeling and validation. *Comput Geotech* 44:116–131
- Guo P, Xiao Y, Kunnath S (2014) Performance of laterally loaded h-piles in sand. *Soil Dyn Earthq Eng* 67:316–325
- Heidari M, Naggari HE, Jahanandish M, Ghahramani A (2014) Generalized cyclic p-y curve modeling for analysis of laterally loaded piles. *Soil Dyn Earthq Eng* 63:138–149
- Ilyas T, Leung CF, Chow YK, Budi SS (2004) Centrifuge model study of laterally loaded pile groups in clay. *J Geotech Geoenviron* 130(3): 274–283
- Larsson S, Malm R, Charbit B, Ansell A (2012) Finite element modelling of laterally loaded lime-cement columns using a damage plasticity model. *Comput Geotech* 44:48–57
- Law HK, Lam IP (2001) Application of periodic boundary for large pile group. *J Geotech Geoenviron* 127(10):889–892
- Loria AFR, Vadrot A, Laloui L (2018) Analysis of the vertical displacement of energy pile groups. *Geomech Energy Environ* 16:1–14
- Mamoon SM, Kaynia AM, Banerjee PK (1990) Frequency domain dynamic analysis of piles and pile groups. *J Eng Mech* 116(10):2237–2257
- Matlock H, Ingram WB, Kelley AE, Bogard D et al (1980) Field tests of the lateral-load behavior of pile groups in soft clay. In *Offshore Technology Conference*. Offshore Technology Conference, Houston. <https://doi.org/10.4043/3871-MS>
- McVay M, Casper R, Shang T-I (1995) Lateral response of three-row groups in loose to dense sands at 3d and 5d pile spacing. *J Geotech Eng* 121(5):436–441
- McVay M, Shang T, Casper R (1996) Centrifuge testing of fixed-head laterally loaded battered and plumb pile groups in sand. *Geotech Test J* 19(1):41–50
- Meimon Y, Baguelin F, Jezequel J (1986) Pile group behaviour under long time lateral monotonic and cyclic loading. In: *Proceedings, third international conference on numerical methods in offshore piling*. Inst. Francais du Petrole, Nantes, France, pp 285–302
- Moss RES, Caliendo JA, Anderson LR (1998) Investigation of a cyclic laterally loaded model pile group. *Soil Dyn Earthq Eng* 17(7–8): 519–523
- Mylonakis G, Gazetas G (1999) Lateral vibration and internal forces of grouped piles in layered soil. *J Geotech Geoenviron* 125(1):16–25
- Ooi PS, Chang BK, Wang S (2004) Simplified lateral load analyses of fixedhead piles and pile groups. *J Geotech Geoenviron* 130(11): 1140–1151
- Padron L, Aznarez J, Maeso O (2007) Bem-fem coupling model for the dynamic analysis of piles and pile groups. *Eng Anal Bound Elem* 31(6):473–484
- Papadopoulou MC, Comodromos EM (2010) On the response prediction of horizontally loaded fixed-head pile groups in sands. *Comput Geotech* 37(7–8):930–941
- Randolph MF, Wroth CP (1979) An analysis of the vertical deformation of pile groups. *Geotechnique* 29(4):423–439
- Rollins KM, Peterson KT, Weaver TJ (1998) Lateral load behavior of full-scale pile group in clay. *J Geotech Geoenviron* 124(6):468–478
- Rollins KM, Olsen RJ, Egbert JJ, Jensen DH, Olsen KG, Garrett BH (2006) Pile spacing effects on lateral pile group behavior: load tests. *J Geotech Geoenviron* 132(10):1262–1271
- Salgado R, Tehrani F, Prezzi M (2014) Analysis of laterally loaded pile groups in multilayered elastic soil. *Comput Geotech* 62:136–153
- Sen R, Davies TG, Banerjee PK (1985) Dynamic analysis of piles and pile groups embedded in homogeneous soils. *Earthq Eng Struct Dyn* 13(1):53–65
- Sun K (1994) A numerical method for laterally loaded piles. *Comput Geotech* 16(4):263–289
- Tahghighi H, Konagai K (2007) Numerical analysis of nonlinear soil-pile group interaction under lateral loads. *Soil Dyn Earthq Eng* 27(5): 463–474
- Wu G, Finn WL, Dowling J (2015) Quasi-3d analysis: validation by full 3d analysis and field tests on single piles and pile groups. *Soil Dyn Earthq Eng* 78:61–70
- Xu KJ, Poulos HG (2000) General elastic analysis of piles and pile groups. *Int J Numer Anal Methods Geomech* 24(15):1109–1138
- Yang Z, Jermic B (2003) Numerical study of group effects for pile groups in sands. *Int J Numer Anal Methods Geomech* 27(15): 1255–1276